Hindawi
Shock and Vibration
Volume 2018, Article ID 5369281, 10 pages
https://doi.org/10.1155/2018/5369281

Research Article

Evaluation of the Wind-Resistant Performance of Long-Span Cable-Stayed Bridge Using the Monitoring Correlation between the Static Cross Wind and Its Displacement Response

Gaoxin Wang[1], **Youliang Ding**[2], **Dongming Feng**[3] and **Jihong Ye**[1]

[1]*State Key Laboratory for Geomechanics and Deep Underground Engineering, China University of Mining and Technology, Xuzhou 221116, China*
[2]*The Key Laboratory of Concrete and Prestressed Concrete Structures of Ministry of Education, Southeast University, Nanjing 210096, China*
[3]*Department of Civil Engineering and Engineering Mechanics, Columbia University, New York, NY 10027, USA*

Correspondence should be addressed to Youliang Ding; 101010916@seu.edu.cn

Received 8 April 2018; Revised 7 July 2018; Accepted 1 August 2018; Published 27 August 2018

Academic Editor: Carlo Rainieri

The wind-resistant performance of existing long-span cable-stayed bridge structures will inevitably deteriorate due to concrete carbonation, reinforcement corrosion, accumulated fatigue damage, etc., which can threaten the entire bridge safety. However, few studies currently focus on assessing the wind-resistant performance of existing long-span cable-stayed bridge structures, and at present, no studies have revealed how to identify the deterioration of the wind-resistant performance using a bridge health-monitoring technique. Therefore, based on the health-monitoring system installed on the Sutong Cable-stayed Bridge, the monitoring wind field and GPS displacement are captured to analyze the wind-resistant performance. First, the correlation between static cross wind and transversal displacement is analyzed, which is nearly linear but also contains discrete points caused by environmental noise. Second, considering that the discrete points can decrease the identification accuracy, one new method called the cross-correlation analysis of wavelet packet coefficients is put forward to effectively remove the discrete points. Third, considering that the traditional function cannot match the monitoring correlation very well, some new fitting functions are thoroughly studied to determine the best function for fitting the monitoring correlation. Fourth, the abnormal variation in the monitoring correlation caused by a deterioration in the wind-resistant performance is studied, and the root-mean-square (RMS) variable, which represents the difference between a good service state and a deteriorated service state, is used as a detection indicator to identify the deterioration of wind-resistant performance. Finally, the monitoring data from ten months are selected to evaluate the wind-resistant performance of the Sutong Bridge, and the result shows that its wind-resistant performance was still in a good service state during these ten months.

1. Introduction

The wind-resistant performance of existing bridge structures will inevitably deteriorate due to the influence from synthetic factors, such as concrete carbonation, reinforcement corrosion, and accumulated fatigue damage, which can threaten the entire bridge safety [1–5]. For example, the boundary beam of the SR1014 Bridge in Pennsylvania laterally collapsed mainly due to serious performance deterioration [5]. Additionally, according to the relevant investigation results [5], the percentage of American bridges that have collapsed due to performance deterioration (mainly including steel brittle fracture, accumulated fatigue damage, and prestressed reinforcement corrosion) is 18.75%. The actual service life of bridges under real environment is usually lower than their designed life (i.e., 100 years) because of performance deterioration. Therefore, it is meaningful to research the deterioration behavior of bridges throughout their service life, which can help prevent bridge failure. Until now, studies on the theoretical exploration and numerical simulations of the

deterioration mechanism have been extensively conducted for concrete bridge structures [1,6–12]. For example, Professor Shi chose a simply supported plate girder as a research object and studied the relationship between the material parameters and failure function through a sensitivity analysis [10]; Ye et al. researched the performance evolution of one continuous concrete box girder by changing the damage time and damage amount [11]; Tian et al. analyzed the performance variation of a continuous concrete girder under chloride penetration environment through finite-element simulation [12]; and Xue et al. explored the ultimate bearing capacity of one continuous rigid-frame bridge based on nonlinear simulation of the concrete material [1].

However, the traditional methods based on theoretical deductions and numerical simulations cannot necessarily accurately represent the real deterioration process at the bridge site because of uncertain boundary conditions, imprecise assignments of initial parameters, and an improper ignorance of subordinate factors. In recent years, with the development of structural health monitoring, massive amounts of monitoring data (wind velocity, acceleration, strain, temperature, displacement, etc.) from bridge structures can be used to assess bridge performance [9,13–17]. For example, Liu et al. collected long-term monitoring strain data induced by heavy vehicle traffic on an existing bridge and then presented a series-parallel system model for a performance assessment [17]. However, few studies have specifically focused on assessing the wind-resistant performance of cable-stayed bridge structures using the bridge health-monitoring technique, and at present, no studies have revealed how to identify the deterioration of the wind-resistant performance of existing cable-stayed bridge structures.

Therefore, this study focuses on evaluating the wind-resistant performance of existing cable-stayed bridge structures using the bridge health-monitoring technique. The basic idea of this research is that the transversal displacement response of the main girder under cross wind relates to the wind-resistant performance, so the wind-resistant performance can be estimated using the correlation between the transversal displacement response and the cross wind. In other words, the abnormal variation of the correlation indicates a deterioration in the wind-resistant performance. Using the monitoring wind field and the GPS displacement of the Sutong Cable-stayed Bridge, one new detailed method called the cross-correlation analysis of wavelet packet coefficients is invented in this research to accurately obtain the correlation between the transversal displacement and the cross wind. The root-mean-square (RMS) variable representing the difference between a good service state and a deteriorated service state of the wind-resistant performance is then used as a detection indicator to evaluate the wind-resistant performance, and finally, the wind-resistant performance of the Sutong Cable-stayed Bridge in the service period is evaluated using the monitoring RMS value.

2. Monitoring Data Analysis

2.1. Description of Bridge Health Monitoring. The monitoring bridge object for this research is the long-span Sutong Cable-stayed Bridge across the Yangtze River as shown in Figure 1, which was the longest cable-stayed bridge in the world when it was open to traffic in May 2008. The main span of this bridge is 1088 m, and the structural type of the main girder is the flat steel box girder as shown in Figure 2. The complexity, scale, and design technology of this project rank first in the history of China. One obvious feature of this bridge is the low stiffness and long natural vibration period, making this bridge very sensitive to wind load [18, 19]. Therefore, the wind-resistant performance of this bridge is thoroughly studied using the monitoring wind load and its displacement response data.

In detail, one 3D ultrasonic anemometer (3DUA) is installed at the upstream side of the main span as shown in Figures 1 and 2 to record the wind load data, which include wind velocity, wind direction angle, and wind attack angle in the local bridge coordinate system (x, y, z), as shown in Figure 3. This ultrasonic anemometer can accurately record the wind speed ranging from 0 m/s to 65 m/s with a resolution of 0.01 m/s and the wind direction angle ranging from 0° to 359.9° with a resolution of 0.1°. Besides, the upper frequency limit can reach 32 Hz, and in this research, the sampling frequency is set as 1 Hz because only the static wind component is mainly concerned. With regard to the wind direction angle, the positive direction of x-axis is defined as 0° and the positive direction rotates clockwise; with regard to the wind attack angle, the z-axis upward is defined as 90° and the direction in the horizontal plane is defined as 0°.

Moreover, the real-time kinematic global positioning system (RTK-GPS) device is employed to record the relative 3D positions of the rovers (i.e., the mobile stations) with respect to the base (i.e., the reference station) in the geographic coordinate system (X, Y, Z), as shown in Figure 3 [20–22]. The estimation accuracy of relative 3D positions can be improved by double-difference calculation of carrier phases from the base and rovers [20, 22]. In detail, the determination steps of relative 3D positions can be summarized as follows [23, 24]: (1) the reference station continuously observes all the GPS satellites and returns real-time monitoring data to the mobile station; (2) the mobile stations receive the observed data from the reference station through radio-receiving equipment while receiving GPS satellite signals as well; (3) the real-time calculations of the baseline vector between reference and mobile stations are conducted, and the coordinates of the mobile station are further obtained by summing the coordinates of the reference station and baseline vector together; and (4) the coordinates of the reference station and mobile station are calculated under the WGS84 coordinate system, so the coordinates of the reference station and mobile station are further projected onto the North-East-Depth geographic coordinate system (X, Y, Z); finally, the relative 3D positions of mobile stations with respect to the reference station in the geographic coordinate system are obtained according to the principle of relative positioning.

In this bridge health-monitoring system, the RTK-GPS contains two GPS receivers (i.e., one base and one rover). The rover is installed at the upstream side of the main span as

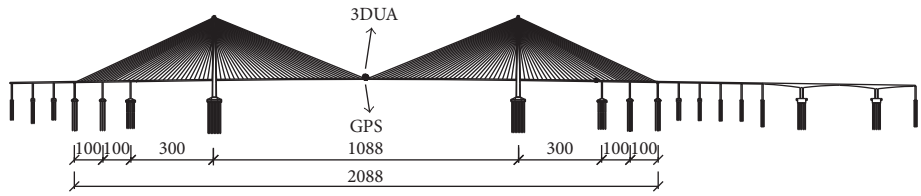

Figure 1: The longitudinal view of the Sutong Cable-stayed Bridge (unit: m).

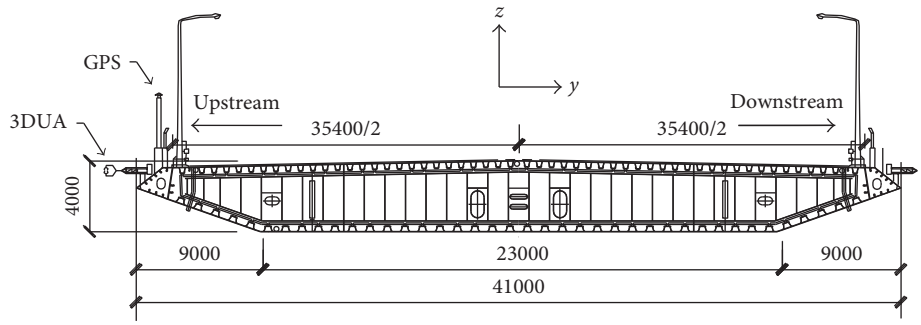

Figure 2: The locations of the 3DUA and GPSMS in the flat steel box girder (unit: mm).

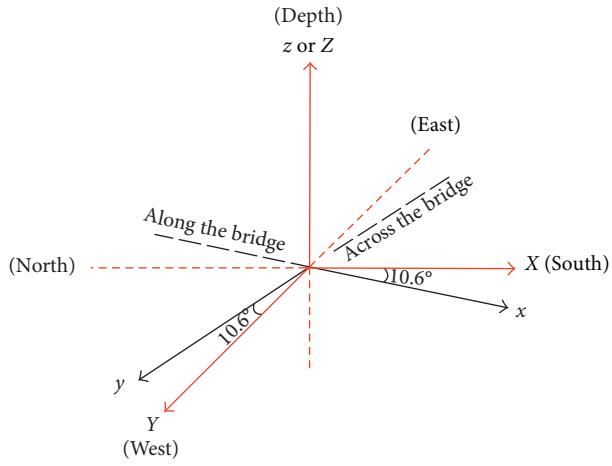

Figure 3: Illustration of the geographic coordinate system (X, Y, Z) and local bridge coordinate system (x, y, z).

shown in Figures 1 and 2, and the base is installed on the roof of the bridge management building near the bridge site. The base serves as a stationary checkpoint whose coordinates have been previously determined by conventional static GPS methods and constantly records the difference between its known position and the position calculated from the satellite data [24]. The sampling frequency of relative 3D positions is set as 1 Hz.

2.2. Monitoring Result. The monitoring data from one month are used for analysis. The monitoring wind data, which include wind velocity, wind direction angle, and wind attack angle, are decomposed to obtain the cross-wind velocity along the y-axis using the skew wind decomposition method [25]:

$$V_c = V \cos\beta \sin\delta, \tag{1}$$

where V_c denotes the cross-wind velocity along the y-axis, V denotes the monitoring wind velocity, β denotes the monitoring wind direction angle, and δ denotes the monitoring wind attack angle. Then, the 10-minute moving average process, which can be considered as one low-pass filter [26], is carried out to remove the dynamic displacement component and obtain the static cross-wind velocity V_s along the y-axis as shown in Figure 4(a). It can be seen that the maximum static cross-wind velocity is 23.92 m/s and the minimum static cross-wind velocity is −12.75 m/s, indicating that obvious static cross-wind velocity exists at the bridge site.

Moreover, it can be seen that the local bridge coordinate system x-y-z and the geographic coordinate system X-Y-Z are not the same; i.e., there is one included angle about 10.6° between the X- and x-axes. Therefore, the relative 3D positions in the geographic coordinate system are decomposed to obtain the transversal bridge displacement along the y-axis through coordinate transformation as follows:

$$D_T = D_X \sin\alpha - D_Y \cos\alpha, \tag{2}$$

where D_T denotes the transversal displacement along the y-axis; D_X and D_Y denote the relative displacements along the X- and Y-axes, respectively; and α denotes the included angle between the X- and x-axes. Then, the 10-minute moving average process is conducted to remove the dynamic displacement component and obtain the static transversal displacement data D_s along the y-axis, as shown in Figure 4(b). It can be seen that the maximum static transversal displacement is 0.259 m, while the minimum static transversal displacement is −0.082 m, indicating that an obvious transversal displacement exists in the Sutong Cable-stayed Bridge under static cross-wind velocity.

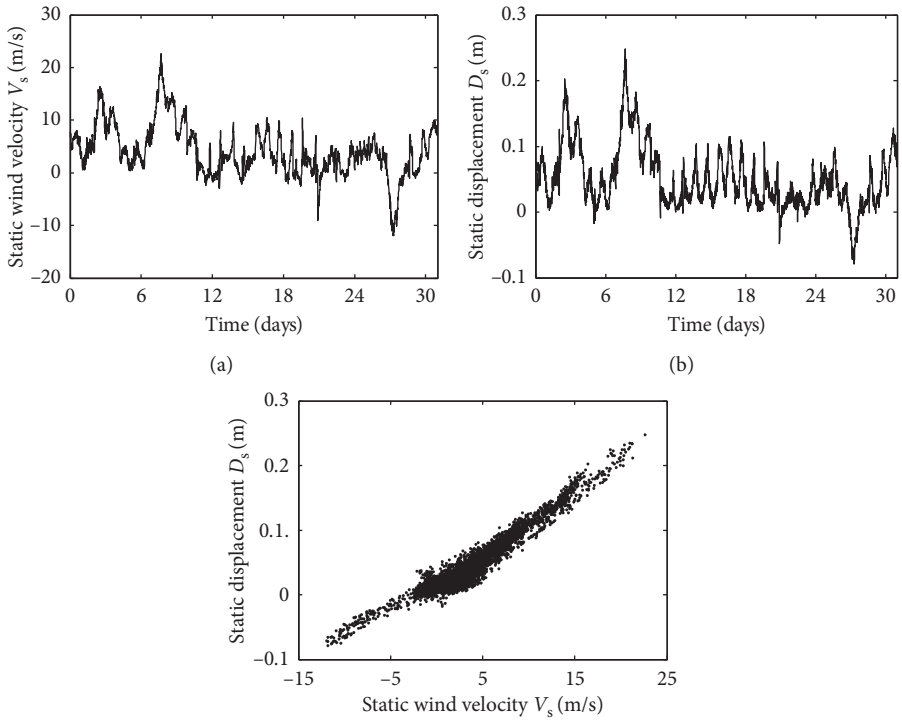

Figure 4: Time histories of V_s and D_s, and the correlation between V_s and D_s: (a) time history of the static cross-wind velocity V_s; (b) time history of the static transversal displacement D_s; (c) the correlation between V_s and D_s.

By comparing V_s and D_s, it is clear that they have similar trends. Accordingly, the correlation between V_s and D_s is plotted in Figure 4(c). It can be seen that V_s clearly increases as D_s increases, and the increasing trend appears to be nearly linear. Additionally, the correlation contains discrete points, which are caused by noise from the environment. Here, the increasing trend is treated as the principal component, and the discrete points are treated as the discrete component. The principal component plus the discrete component is the total trend of the correlation.

3. Principal Component Analysis

The discrete points have a negative influence on the estimation accuracy of the wind-resistant performance, so it is necessary to decrease the amount of discrete points. One new method referred to as a cross-correlation analysis of wavelet packet coefficients (CAWPC) is introduced to effectively remove the discrete component while extracting the principal component from the correlation.

3.1. Analysis Method. The basic idea of the CAWPC method contains three parts:

Part 1: to more easily conduct the analysis, the correlation in Figure 4 is divided into several segments, as shown in Figure 5. The correlations in each segment are considered to be linear, so the correlations are treated as combinations of linear segments.

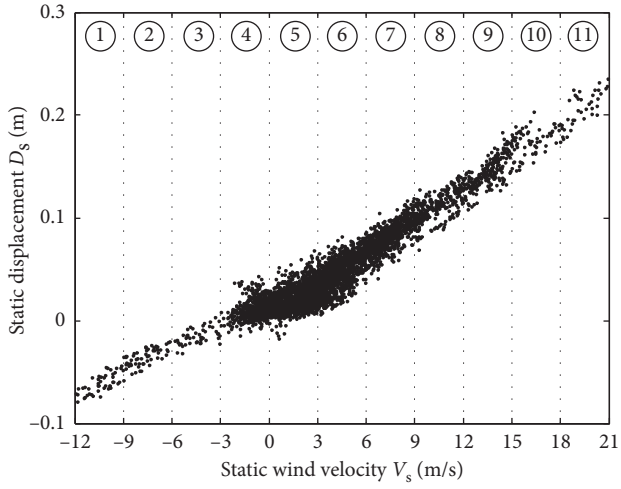

Figure 5: Eleven segments of the correlation.

Part 2: the correlation in each segment contains a principal component as well as a discrete component. One distinct difference between the principal component and the discrete component is that the value of D_s caused by V_s in the principal component changes gently, but the value of D_s caused by V_s in the discrete component clearly fluctuates; so the principal component and discrete component have different frequency bands. Therefore, the wavelet packet method is introduced to decompose D_s and V_s in each segment

into different frequency bands. Based on a pair of low-pass and high-pass conjugate quadrature filters $h(j)$ and $g(j)$ of the wavelet packet [27, 28], D_s or V_s in each segment can be decomposed scale by scale into different frequency bands. In each frequency band, one corresponding decomposition coefficient is obtained, which is calculated as follows [29]:

$$C_p^{i,2l} = \sum_{q \in Z} C_q^{i+1,l} h(q-2j), \tag{3}$$

$$C_p^{i,2l+1} = \sum_{q \in Z} C_q^{i+1,l} g(q-2j), \tag{4}$$

where $C_p^{i,2l}$ denotes the decomposition coefficient in the kth frequency band under the $2l$th scale and $C_p^{i,2l+1}$ denotes the decomposition coefficient in the kth frequency band under the $(2l+1)$th scale.

Part 3: after the wavelet packet decomposition, D_s and V_s in each segment have many decomposition coefficients, and each decomposition coefficient from D_s corresponds to one decomposition coefficient from V_s in the same frequency band, i.e., a pair of decomposition coefficients. Some pairs of decomposition coefficients mainly contain the principal component, and the other pairs of decomposition coefficients mostly contain the discrete component; so the pairs of decomposition coefficients containing the principal component should be selected from all the decomposition coefficients. Each decomposition coefficient can be reconstructed into one time-domain signal. If one pair of decomposition coefficients contains a principal component, their reconstructed time-domain signals should have good linear cross-correlation characteristics to each other, which can be judged by the following formula:

$$c = \frac{\sum_{m=1}^{n} (V_R^m - \overline{V})_R \left(|D_R^m| - |\overline{D}_R| \right)}{\left[\sum_{m=1}^{n} (V_R^m - \overline{V}_R)^2 \sum_{m=1}^{n} \left(|D_R^m| - |\overline{D}_R| \right)^2 \right]^{0.5}}, \tag{5}$$

where c denotes the linear cross-correlation coefficient of the reconstructed time-domain signals of D_s and V_s; V_R^m and D_R^m denote the mth values in the reconstructed time-domain signals of V_s and D_s, respectively; $\overline{V}_R$ and $\overline{D}_R$ denote the average values of V_R^m and D_R^m, respectively; and n denotes the total amount of V_R^m or D_R^m. Therefore, if the calculation result of c is close to 1, it can be concluded that the reconstructed time-domain signals of D_s and V_s have good linear cross-correlation characteristics to each other, so the corresponding pair of decomposition coefficients is retained. Otherwise, if the calculation result of c is close to 0, the corresponding pair of decomposition coefficients is removed. Finally, after cross-correlation analysis, only the pairs of decomposition coefficients containing the principal component are retained. Therefore, the reconstructed time-domain signals of D_s and V_s mainly contain the principal component.

3.2. Analysis Steps. In detail, this CAWPC method is carried out by the following four steps:

(1) The correlation between V_s and D_s is divided into w segments, as shown in Figure 5. The correlation in each segment contains a principal component as well as a discrete component. The static wind velocity and static displacement in the kth segment are denoted by $V_{s,k}$ and $D_{s,k}$, respectively, where $k = 1, 2, \ldots, w$.

(2) $V_{s,k}$ and $D_{s,k}$ are each decomposed into 2^s frequency bands using the wavelet packet method. In each frequency band, the corresponding decomposition coefficients are obtained. The jth decomposition coefficient of $V_{s,k}$ is reconstructed into the time-domain static wind velocity V_k^j, and the jth decomposition coefficient of $D_{s,k}$ is reconstructed into the time-domain static displacement D_k^j, where $j = 1, 2, \ldots, 2^s$. The jth decomposition coefficients of $V_{s,k}$ and $D_{s,k}$ are the jth pair of decomposition coefficients in the jth frequency band.

(3) Based on (4), the linear cross-correlation coefficient of V_k^j and D_k^j, which is denoted by c_k^j, is calculated to judge whether the correlation between V_k^j and D_k^j contains good linear characteristics:

$$c_k^j = \frac{\sum_{m=1}^{n} \left(V_k^{j,m} - \overline{V}_k^j \right) \left(D_k^{j,m} - \overline{D}_k^j \right)}{\left[\sum_{m=1}^{n} \left(V_k^{j,m} - \overline{V}_k^j \right)^2 \sum_{m=1}^{n} \left(D_k^{j,m} - \overline{D}_k^j \right)^2 \right]^{0.5}}, \tag{6}$$

where $V_k^{j,m}$ and $D_k^{j,m}$ denote the mth values of V_k^j and D_k^j, respectively, and $\overline{V}_k^j$ and D_k^j denote the average values of V_k^j and D_k^j, respectively. If the calculation result of c_k^j is close to 1, it can be concluded that V_k^j and D_k^j have good linear cross-correlation characteristics, so the jth pair of decomposition coefficients is retained; otherwise, the jth pair of decomposition coefficients is removed.

(4) After cross-correlation analysis, only the pairs of decomposition coefficients containing good linear cross-correlation characteristics are retained. Then, all the reconstructed time-domain static wind velocity data V_k^j from the remaining decomposition coefficients are superposed to obtain the static wind velocity $\widetilde{V}_{s,k}$ in the kth segment, and all the reconstructed time-domain static displacement data D_k^j from the remaining decomposition coefficients are superposed to obtain the static displacement data $\widetilde{D}_{s,k}$ in the kth segment. The correlation between $\widetilde{V}_{s,k}$ and $\widetilde{D}_{s,k}$ mainly contains the principal component in the kth segment. Furthermore, the principal components from all the segments constitute the principal component of the whole correlation between V_s and D_s; that is, $\widetilde{V}_s = [\widetilde{V}_{s,1}, \widetilde{V}_{s,2}, \ldots, \widetilde{V}_{s,w}]$ and $\widetilde{D}_s = [\widetilde{D}_{s,1}, \widetilde{D}_{s,2}, \ldots, \widetilde{D}_{s,w}]$.

3.3. Results. According to the four steps mentioned above, the parameter values of w and s in the CAWPC method during analysis are set to 11 and 8, respectively. The principal component of the correlation between V_s and D_s from Figure 4 is further extracted and shown in Figure 6. It can be seen that, after the CAWPC analysis, the principal component obviously presents a nearly linearly increasing trend with few discrete points compared to that in Figure 4(c), verifying that the CAWPC method is effective and can be further used for evaluating the wind-resistant performance.

4. Evaluation Method Analysis

At the beginning of the service period, the Sutong Bridge had a good wind-resistant performance. However, as the service time increases, the wind-resistant performance will inevitably deteriorate due to the influence of synthetic factors, such as concrete carbonation, reinforcement corrosion, and accumulated fatigue damage. The transversal displacement response of the main girder under cross winds relates to the wind-resistant performance, so the wind-resistant performance can be estimated using the correlation between the transversal displacement response and the cross wind; in other words, the abnormal variation of the correlation indicates a deterioration in the wind-resistant performance.

4.1. Deterioration Process of Wind-Resistant Performance. The static cross-wind load F relates to the static wind velocity $\widetilde{V}_s$, which can be expressed as follows [30]:

$$F = 0.5\rho C_H H \widetilde{V}_s^2, \tag{7}$$

where ρ is the air density, C_H is the resistance coefficient, and H is the projection height of the flat steel box girder. Furthermore, the static displacement response $\widetilde{D}_s$ is induced by the static cross-wind load F, which can be modeled using one second-order polynomial function (abbreviated as TPF) as follows [31]:

$$\widetilde{D}_{s\,\mathrm{TPF}} = F\delta = 0.5\rho C_H H\delta \widetilde{V}_s^2 = 0.5\rho C_H H\delta \widetilde{V}_s^2, \tag{8a}$$

$$\text{or} \quad \left|\widetilde{D}_s\right|_{\mathrm{TPF}} = 0.5\rho C_H H\delta \left|\widetilde{V}_s\right|^2, \tag{8b}$$

where $\widetilde{D}_{s\,\mathrm{TPF}}$ denotes the static displacement $\widetilde{D}_s$ in the function TPF, $|\widetilde{D}_s|_{\mathrm{TPF}}$ denotes the absolute static displacement $|\widetilde{D}_s|$ in the function TPF, and δ denotes the wind-resistant flexibility of the Sutong Bridge. According to (8b), the static displacement response $\widetilde{D}_s$ should be 0 if the static wind velocity $\widetilde{V}_s$ is 0, so the monitoring correlation between $\widetilde{D}_s$ and $\widetilde{V}_s$ is shifted along the horizontal axis to meet this condition. Then, (8b) is fitted using the monitoring correlation between $|\widetilde{V}_s|$ and $|\widetilde{D}_s|$ in the least-squares sense. Before fitting (8b), the monitoring correlations between $|\widetilde{V}_s|$ and $|\widetilde{D}_s|$ are divided into two parts: the monitoring correlation within the wind velocity intervals [0 m/s, 15 m/s] is used as training data to fit (8b), and the monitoring correlation within the wind velocity intervals (15 m/s, 24 m/s] is used as test data to verify the fitting results of (8a). After the least-squares analysis, the fitted result of (8b) is $|\widetilde{D}_s| = 0.00071|\widetilde{V}_s|^2$, as shown in Figure 7. It can be seen that the fitted result of (8b) does not match the monitoring correlation very well in the test phase. Therefore, more possible functions, including the power function (PF), Fourier function (FF), fourth-order polynomial function (FPF), sine function (SF), and Gauss function (GF), are concretely studied to fit the monitoring correlation. Using the mathematical functions PF, FF, FPF, SF, and GF to fit the in situ data belongs to the data-driven method, which has been commonly used in current research [32, 33]. According to the definition of this method, although this method does not contain the basic physical meaning regarding the relation between displacement and wind velocity, the calculated results are equivalent to the real physical model if the mathematical functions are well fitted. These mathematical equations are expressed as follows.

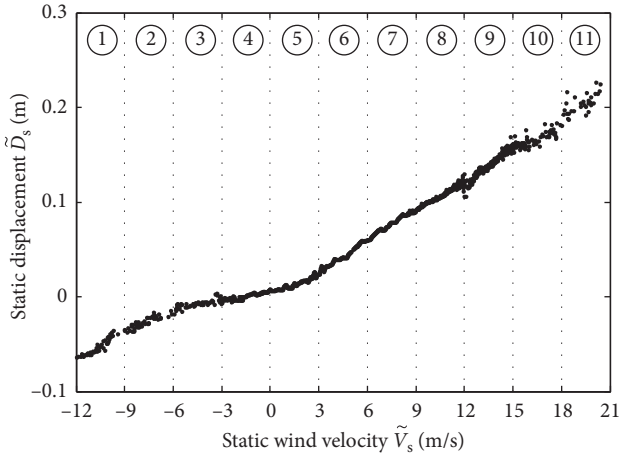

Figure 6: The principal component of the correlation.

(1) Power function (PF):

$$\left|\widetilde{D}_s\right|_{\mathrm{PF}} = a\left|\widetilde{V}_s\right|^b, \tag{9a}$$

where $|\widetilde{D}_s|_{\mathrm{PF}}$ denotes the static displacement $|\widetilde{D}_s|$ in the function PF, and a and b denote the parameters to be estimated in the function PF.

(2) Fourier function (FF):

$$\left|\widetilde{D}_s\right|_{\mathrm{FF}} = a_0 + \sum_{i=1}^{4}\left(a_i \cos wi\left|\widetilde{V}_s\right| + b_i \sin wi\left|\widetilde{V}_s\right|\right), \tag{9b}$$

where $|\widetilde{D}_s|_{\mathrm{FF}}$ denotes the static displacement $|\widetilde{D}_s|$ in the function FF, and $a_0, a_1, \ldots, a_4$ and $b_1, b_2, \ldots, b_4$ denote the parameters to be estimated in the function FF.

(3) Fourth-order polynomial function (FPF):

$$\left|\widetilde{D}_s\right|_{\mathrm{FPF}} = \sum_{i=0}^{4} p_i\left|\widetilde{V}_s\right|^i, \tag{9c}$$

where $|\widetilde{D}_s|_{\mathrm{FPF}}$ denotes the static displacement $|\widetilde{D}_s|$ in the function FPF, and $p_0, p_1, \ldots, p_4$ denote the parameters to be estimated in the function FPF.

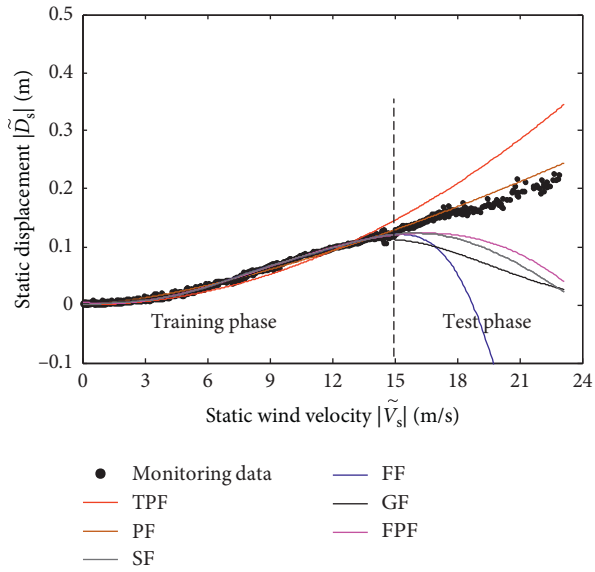

Figure 7: The fitted results of the monitoring correlation.

(4) Sine function (SF):

$$\left|\tilde{D}_s\right|_{SF} = \sum_{i=1}^{4} a_i \sin\left(b_i\left|\tilde{V}_s\right| + c_i\right), \tag{9d}$$

where $|\tilde{D}_s|_{SF}$ denotes the static displacement $|\tilde{D}_s|$ in the function SF, and $a_1, a_2, \ldots, a_4, b_1, b_2, \ldots, b_4$, and $c_1, c_2, \ldots, c_4$ denote the parameters to be estimated in the function SF.

(5) Gauss function (GF):

$$\left|\tilde{D}_s\right|_{GF} = \sum_{i=1}^{4} a_i e^{\left(\tilde{V}_s - b_i/c_i\right)^2}, \tag{9e}$$

where $|\tilde{D}_s|_{GF}$ denotes the static displacement $|\tilde{D}_s|$ in the function GF, and $a_1, a_2, \ldots, a_4, b_1, b_2, \ldots, b_4$, and $c_1, c_2, \ldots, c_4$ denote the parameters to be estimated in the function GF.

After the least-squares analysis, the fitted results of all the functions are shown in Figure 7. It can be seen that although all the fitted functions match the monitoring correlation well in the training phase, only the power function (PF) matches the monitoring correlation well in the test phase, so the power function (PF) is selected to represent the monitoring correlation, with the estimated values of a and b in the PF at 0.002374 and 1.476, respectively.

Furthermore, the static displacement $|\tilde{D}_s|_{PF}$ in (8a) is induced by the static cross-wind load F, which can be expressed as follows:

$$\left|\tilde{D}_s\right|_{PF} = F\delta. \tag{10}$$

Suppose that the wind-resistant performance of the Sutong Bridge gradually deteriorates in the service period, and the deterioration amount is $\Delta\delta$. Then, the static displacement $|\hat{D}_s|$ after deterioration can be reexpressed as follows:

$$\left|\hat{D}_s\right| = F(\delta + \Delta\delta) = \left(1 + \frac{\Delta\delta}{\delta}\right) a\left|\tilde{V}_s\right|^b. \tag{11}$$

Taking the principal component in Figure 6 as an example, if $\Delta\delta = 0$, 0.3δ, and 0.6δ, respectively, the deterioration results of the principal component corresponding to different $\Delta\delta$ values are shown in Figure 8(a). It can be seen that the principal component obviously deviates from its good service state during deterioration, and the principal component gradually becomes thinner as the deterioration amount $\Delta\delta$ increases. What should be emphasized here is that the CAWPC method plays one important role in obtaining the distinct deterioration of the wind-resistant performance in Figure 8(a). If the correlation between $|V_s|$ and $|D_s|$ in Figure 4(c), which does not undergo CAWPC analysis, is used to analyze the deterioration of the wind-resistant performance as shown in Figure 8(b), it can be seen that the deterioration of wind-resistant performance is fuzzy compared with that in Figure 8(a), which can obviously decrease the identification accuracy of deterioration identification.

4.2. Method of Deterioration Identification. As mentioned above, the principal component will gradually deviate from its good service state during deterioration as shown in Figure 8(a), and the deviation amount can be used to identify the deterioration of the wind-resistant performance. The deviation amount can be concretely described using the root-mean-square (RMS) value, which represents the difference between a good service state and a deteriorated service state. Specifically, the steps of deterioration identification of the wind-resistant performance are shown as follows:

(1) The monitoring data of the static cross-wind velocity and its transversal displacement response are divided by months. The principal component of the correlation between the static cross-wind velocity and the transversal displacement in each month is extracted through CAWPC analysis. Suppose that the principal component in the first month corresponds to the good service state of wind-resistant performance, which is mathematically modeled by (8a).

(2) The principal components of the monitoring correlation in the mth month are denoted by $\tilde{V}_s^m$ and $|\tilde{D}_s^m|$, respectively. $\tilde{V}_s^m$ is substituted into (8a) to obtain $|\hat{D}_s^m|$ as follows:

$$\left|\hat{D}_s^m\right| = a\left|\tilde{V}_s^m\right|^b. \tag{12}$$

The deviation amount between the deteriorated service state and the good service state is calculated by $|\hat{D}_s^m| - |\tilde{D}_s^m|$, and then, the RMS value of $(|\hat{D}_s^m| - |\tilde{D}_s^m|)$ is calculated as follows:

$$R_m = \sqrt{\frac{\sum_{k=1}^{N_m}\left(\left|\hat{D}_s^m(k)\right| - \left|\tilde{D}_s^m(k)\right|\right)^2}{N_m}}, \tag{13}$$

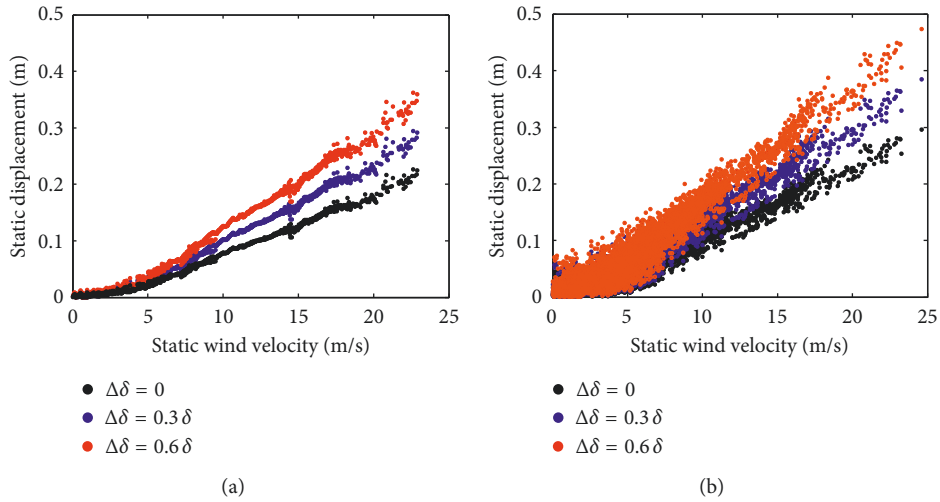

Figure 8: The deterioration of wind-resistant performance: (a) after the cross-correlation analysis; (b) before the cross-correlation analysis.

where R_m denotes the RMS value in the mth month; N_m denotes the total amount of $|\widehat{D}_s^m|$ or $|\widetilde{D}_s^m|$; and $|\widehat{D}_s^m(k)|$ and $|\widetilde{D}_s^m(k)|$ denote the kth values of $|\widehat{D}_s^m|$ and $|\widetilde{D}_s^m|$, respectively.

(3) As mentioned earlier, the principal component will gradually become thinner as the deterioration amount $\Delta\delta$ increases (Figure 8(a)), indicating that the values of R_m will gradually increase with the deterioration process of wind-resistant performance. Therefore, a gradual increase in R_m can indicate the deterioration of the wind-resistant performance.

4.3. Results. According to the three steps mentioned above, the monitoring data of the static cross-wind velocity and its transversal displacement in ten months are used to identify whether or not the wind-resistant performance of the Sutong Bridge is in a good service state. Finally, the calculation results of $R_1, R_1, \ldots, R_{10}$ are shown in Figure 9, which does not present an increasing trend, indicating that the wind-resistant performance of the Sutong Bridge was still in a good service state during these ten months.

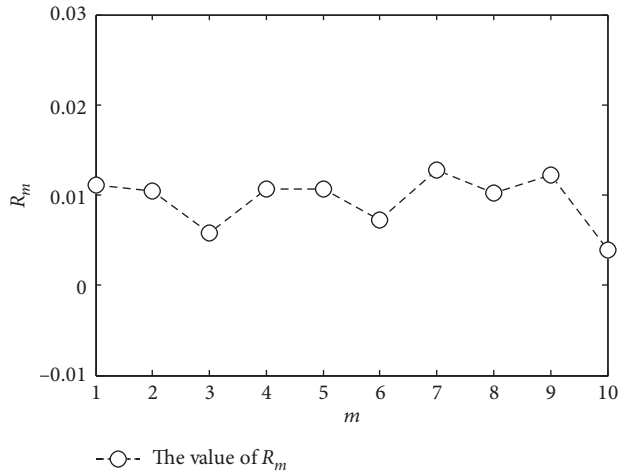

Figure 9: The calculation results of $R_1, R_1, \ldots, R_{10}$.

5. Conclusions

Based on the bridge health-monitoring system, this research conducted a thorough evaluation on the wind-resistant behavior of the Sutong Cable-stayed Bridge using the correlation between the static cross wind and transversal displacement. The following main conclusions were drawn:

(1) The monitoring correlation between the static cross wind and transversal displacement response shows a nearly linearly increasing trend and contains discrete points influenced by environmental noise.

(2) A new method called the cross-correlation analysis of wavelet packet coefficients (CAWPC) can effectively remove the discrete points from the monitoring correlation.

(3) After a comparison of many fitted functions, the fitted power function (PF) can match the monitoring correlation best in both the training and test phases, so the PF is selected to represent the monitoring correlation.

(4) The deterioration process of wind-resistant performance related to the abnormal variation of the correlation is revealed, and additionally, the root-mean-square variable, which represents the difference between a good service state and a deteriorated service state, is put forward to identify the deterioration of wind-resistant performance;

(5) The monitoring data from ten months are selected to evaluate the wind-resistant performance of the Sutong Bridge, and finally, the result shows that the Sutong Cable-stayed Bridge maintained a good service state during these ten months.

What should be mentioned is that the deterioration process of wind-resistant performance is long-term and

slow, so ten-month monitoring data may not contain obvious deterioration information. Hence, our bridge health-monitoring system will continuously monitor the Sutong Bridge, and more monitoring data in the future will be used to judge the wind-resistant performance of the Sutong Bridge.

Data Availability

The datasets generated during the current study are not publicly available but are available from the corresponding author on reasonable request.

Conflicts of Interest

The authors declare that there are no conflicts of interest regarding the publication of this paper.

Acknowledgments

The authors gratefully acknowledge the Fundamental Research Funds for the Central Universities (2018QNA37).

References

[1] P. F. Xue, D. L. Mao, and J. F. Wang, "The ultimate bearing capacity analysis of P.C. bridge based on material performance," *Advanced Materials Research*, vol. 163–167, pp. 3391–3400, 2011.

[2] Y. Liu, X. F. Yin, L. Deng, and C. S. Cai, "Ride comfort of the bridge-traffic-wind coupled system considering bridge surface deterioration," *Wind and Structures*, vol. 23, no. 1, pp. 19–43, 2016.

[3] W. W. Guo, H. Xia, R. Karoumi, T. Zhang, and X. Li, "Aerodynamic effect of wind barriers and running safety of trains on high-speed railway bridges under cross winds," *Wind and Structures*, vol. 20, no. 2, pp. 213–236, 2015.

[4] S. J. W. Bush, T. F. P. Henning, A. Raith, and J. M. Ingham, "Development of a bridge deterioration model in a data-constrained environment," *Journal of Performance of Constructed Facilities*, vol. 31, no. 5, article 04017080, 2017.

[5] L. Sun and Z. Liu, "Case analysis and lessons drawn from bridge failures in United States from 2000 to 2008," *World Bridges*, no. 3, pp. 46–49, 2009, in Chinese.

[6] Q. Chun and L. X. Sun, "Structural performance analysis and repair design of Wenxing Lounge Bridge," *Advanced Materials Research*, vol. 778, pp. 1014–1019, 2013.

[7] S. L. Li, Y. Xu, S. Y. Zhu, X. C. Guo, and Y. Q. Bao, "Probabilistic deterioration model of high-strength steel wires and its application to bridge cables," *Structure and Infrastructure Engineering*, vol. 11, no. 9, pp. 1240–1249, 2015.

[8] A. V. Varnavina, L. H. Sneed, A. K. Khamzin, E. V. Torgashov, and N. L. Anderson, "An attempt to describe a relationship between concrete deterioration quantities and bridge deck condition assessment techniques," *Journal of Applied Geophysics*, vol. 142, pp. 38–48, 2017.

[9] H. Tian, G. P. Li, and A. R. Chen, "Deterioration process assessment of prestressed concrete continuous bridges in lifecycle," *Journal of Central South University of Technology*, vol. 19, no. 5, pp. 1411–1418, 2012.

[10] X. F. Shi, X. M. Wang, and X. Ruan, "Failure probability assessment of existing RC beam bridges considering spatial variability," *China Civil Engineering Journal*, vol. 44, no. 6, pp. 74–79, 2011.

[11] W. Y. Ye, G. P. Li, and L. C. Fan, "Evolution analysis on global performance of prestressed continuous bridge in lifetime," *Journal of Chongqing Jiaotong University*, vol. 32, pp. 894–898, 2013, in Chinese.

[12] H. Tian, A. R. Chen, and L. Chen, "Structural performance assessment of concrete bridges in life-cycle," *Journal of Zhejiang University*, vol. 46, no. 1, pp. 53–57, 2012.

[13] A. D. Orcesi and D. M. Frangopol, "Bridge performance monitoring based on traffic data," *Journal of Engineering Mechanics*, vol. 139, no. 11, pp. 1508–1520, 2013.

[14] N. M. Okasha and D. M. Frangopol, "Integration of structural health monitoring in a system performance based life-cycle bridge management framework," *Structure and Infrastructure Engineering*, vol. 8, no. 11, pp. 999–1016, 2012.

[15] J. L. Xia, F. C. Cao, and Y. J. Ge, "Wind resistance performance of a double-slotting suspension bridge and its aerodynamic control measures," *Journal of Vibration and Shock*, vol. 36, no. 10, pp. 69–75, 2017.

[16] Z. W. Yu, Z. Shan, J. Yuan, and X. Li, "Performance deterioration of heavy-haul railway bridges under fatigue loading monitored by a multisensor system," *Journal of Sensors*, vol. 2018, Article ID 5465391, 14 pages, 2018.

[17] M. Liu, D. M. Frangopol, and S. Y. Kim, "Bridge system performance assessment from structural health," *Journal of Structural Engineering*, vol. 135, no. 6, pp. 733–742, 2009.

[18] H. Wang, A. Q. Li, J. Niu, Z. H. Zong, and J. Li, "Long-term monitoring of wind characteristics at Sutong Bridge site," *Journal of Wind Engineering and Industrial Aerodynamics*, vol. 115, pp. 39–47, 2013.

[19] H. Wang, T. Wu, T. Y. Tao, A. Q. Li, and A. Kareem, "Measurements and analysis of non-stationary wind characteristics at Sutong Bridge in Typhoon Damrey," *Journal of Wind Engineering and Industrial Aerodynamics*, vol. 151, pp. 100–106, 2016.

[20] G. Koo, K. Kim, J. Y. Chung et al., "Development of a high precision displacement measurement system by fusing a low cost RTK-GPS sensor and a force feedback accelerometer for infrastructure monitoring," *Sensors*, vol. 17, no. 12, p. 2745, 2017.

[21] G. E. Vazquez, J. R. Gaxiola-Camacho, R. Bennett, G. M. Guzman-Acevedo, and I. E. Gaxiola-Camacho, "Structural evaluation of dynamic and semi-static displacements of the Juarez Bridge using GPS technology," *Measurement*, vol. 110, pp. 146–153, 2017.

[22] R. J. Xi, W. P. Jiang, X. L. Meng, H. Chen, and Q. S. Chen, "Bridge monitoring using BDS-RTK and GPS-RTK techniques," *Measurement*, vol. 120, pp. 128–139, 2018.

[23] C. B. Xiong, H. L. Lu, and J. S. Zhu, "Operational modal analysis of bridge structures with data from GNSS/accelerometer measurements," *Sensors*, vol. 17, no. 3, p. 436, 2017.

[24] T. H. Yi, H. N. Li, and M. Gu, "Recent research and applications of GPS based technology for bridge health monitoring," *Science China-Technological Sciences*, vol. 53, no. 10, pp. 2597–2610, 2010.

[25] L. D. Zhu and F. Y. Xu, "Buffeting response of long-span cable-supported bridges under skew winds. Part 1: theory," *Journal of Sound and Vibration*, vol. 281, no. 3–5, pp. 647–673, 2005.

[26] J. Lee, "Real-time digital signal recovery for a multi-pole low-pass transfer function system," *Review of Scientific Instruments*, vol. 88, no. 8, article 085104, 2017.

[27] C. Mborah and G. Maochen, "Enhancing manual P-phase arrival detection and automatic onset time picking in a noisy microseismic data in underground mines," *International Journal of Mining and Technology*, vol. 28, no. 4, pp. 691–699, 2018.

[28] C. Sheng, C. L. Duan, Y. M. Zhao, L. Dong, and Z. F. Luo, "Analysis and evaluation on pressure fluctuations in air dense medium fluidized bed," *International Journal of Mining and Technology*, vol. 28, no. 3, pp. 461–467, 2018.

[29] S. W. Fei, "Fault diagnosis of bearing based on wavelet packet transform-phase space reconstruction-singular value decomposition and SVM classifier," *Arabian Journal for Science and Engineering*, vol. 42, no. 5, pp. 1967–1975, 2017.

[30] X. Y. Zheng, Y. Xu, and Z. D. Feng, "Performance of long-span multi-tower suspension bridge with the action of static wind," in *Proceedings of International Conference on Electric Technology and Civil Engineering*, Lushan, China, April 2011.

[31] J. Cheng and R. C. Xiao, "A simplified method for lateral response analysis of suspension bridges under wind loads," *Communications in Numerical Methods in Engineering*, vol. 22, no. 8, pp. 861–874, 2006.

[32] J. M. D. Delgado, L. J. Butler, I. Brilakis, M. Z. E. B. Elshafie, and C. R. Middleton, "Structural performance monitoring using a dynamic data-driven BIM environment," *Journal of Computing in Civil Engineering*, vol. 32, no. 3, article 04018009, 2018.

[33] Z. Song, Z. J. Zhang, Y. Jiang, and J. Zhu, "Wind turbine health state monitoring based on a Bayesian data-driven approach," *Renewable Energy*, vol. 125, pp. 172–181, 2018.